Correlations between Interannual SST Oscillations and Modeled Swell Impacts on Turbulent Mixing*

YALIN FAN, W. ERICK ROGERS, AND TOMMY G. JENSEN

Oceanography Division, Naval Research Laboratory, Stennis Space Center, Mississippi

(Manuscript received 1 July 2015, in final form 29 September 2015)

ABSTRACT

The possibility of teleconnections between Southern Ocean swells and sea surface temperature (SST) anomalies on interannual time scales in the eastern Pacific Niño-3 region and southeastern Indian Ocean is investigated using numerical wave models. Two alternative parameterizations for swell dissipation are used. It is found that swell dissipation in the models is not directly correlated with large interannual variations such as El Niño–Southern Oscillation (ENSO) or the Indian Ocean dipole (IOD). However, using one of the two swell dissipation parameterizations, a correlation is found between observed SST anomalies and the modification of turbulent kinetic energy flux (TKEF) by Southern Ocean swells due to the damping of short wind waves: modeled reduction of TKEF is opposite in phase to the SST anomalies in the Niño-3 region, indicating a potential positive feedback. The modeled bimonthly averaged TKEF reduction in the southeastern Indian Ocean is also well correlated with the IOD mode.

1. Introduction

Wind-generated ocean surface gravity waves (wind waves) are present at the interface between the atmosphere and the ocean most times and play a significant role in many physical processes at the air–sea interface, including the transfer of momentum, heat, and moisture (Li and Garrett 1997; Grachev and Fairall 2001; Hanley and Belcher 2008; Fan et al. 2009, 2010; Cavaleri et al. 2012). Recognizing their importance to upper ocean dynamics, modifications have been developed for ocean mixing schemes to incorporate effects from surface ocean waves. A Langmuir turbulence parameterization was proposed by McWilliams and Sullivan (2000) and later improved by Smyth et al. (2002) for large circulation models. It gives apparent improvements to mixed layer dynamics in the fully coupled Geophysical Fluid Dynamics Laboratory (GFDL) global climate model in the mid- and high-latitude regions, while no improvements are found in the equatorial region (Fan and Griffies 2014).

Qiao et al. (2004) suggested that the wave orbital velocity should be included in the calculation of Reynolds stress. Their nonbreaking wave parameterization shows improvements in the midlatitude regions in large circulation models (Qiao et al. 2010; Huang et al. 2011, 2012; Fan and Griffies 2014), but improvements in the equatorial region are also very limited for their method.

This lack of improvement is not surprising because both parameterizations are based on Stokes drift or wave orbital velocities, and the equatorial region is dominated by swells (>90%) throughout the year (Fan et al. 2014). When wind waves leave their generation zone and no longer get energy from the local winds, they are considered swells. Swells have only small contributions to orbital velocities and Stokes drift, so their effect in both parameterizations is negligible.

The tropical Pacific is an important region for El Niño–Southern Oscillation (ENSO), which is the most important pattern of large-scale climate variability in the tropics. It is characterized by increased sea surface temperature (SST) in the tropical eastern Pacific Ocean and air surface pressure anomalies in the tropical western Pacific. The oscillations of this climate pattern cause extreme weather such as floods and droughts in many regions of the world (e.g., Philander

* Office of Naval Research Contribution Number NRL/JA/7320-15-2622.

Corresponding author address: Yalin Fan, Oceanography Division, Naval Research Laboratory, 1009 Balch Blvd., Stennis Space Center, MS 39529.
E-mail: yalin.fan@nrlssc.navy.mil

DOI: 10.1175/JCLI-D-15-0455.1

1990). Yet, the mechanisms that cause ENSO and maintain these conditions for many months remain under study. Fan et al. (2012) noted a well-confined tongue-shaped region of surface waves with large mean wavelength to the west of the South American coast, which coincide with the Niño-3 region and where the eastern Pacific cold tongue exists. They speculated that the interaction between the local winds and these long swells could have an effect on SST and mixed layer depth in these regions.

They also found an area with large swell dominance in the southeastern Indian Ocean, which stands out from the rest of the Indian Ocean. This area is also where the cold SST anomalies emerge for a positive Indian Ocean dipole (IOD). A positive IOD experiences greater than average SST in the northwestern Indian Ocean and increased precipitation in East Africa, with a corresponding cold SST anomaly in the eastern Indian Ocean, causing droughts in adjacent land areas of Indonesia and Australia (Saji et al. 1999; Webster et al. 1999; Murtugudde et al. 2000). The IOD also affects the strength of monsoons over the Indian subcontinent, with enhanced summer monsoon rainfall in positive IOD years and vice versa (Cherchi and Navarra 2013). The motivation for this study were the intriguing results by Fan et al. (2012) that revealed an impact of the Southern Oscillation index and significant wave height in the tropics. This raised the question whether there is a link between swells and SST in those areas of active tropical air–sea interaction.

Waves give up energy and momentum when they dissipate. In the case of breaking waves, this energy and momentum clearly goes to the ocean. However, not all dissipation occurs from breaking, and whether the associated fluxes from nonbreaking waves go up to the atmosphere or down into the ocean is still in debate. In the first case, it is argued that swells can interact with the airflow and create wave-driven winds (Harris 1966). Wave-to-atmosphere momentum flux (WAMF) was observed by Donelan et al. (1997) off the coast of Virginia when swell aligned with the wind. Many cases of WAMF have been observed in the tropical Pacific, where calm-to-light winds are common in the presence of strong swells (Grachev and Fairall 2001). Large-eddy simulation studies conducted by Sullivan et al. (2008) also illustrated this phenomenon of WAMF by wind following swells. In contrast to these ideas, Babanin (2011) and Zieger et al. (2015) argue that the nonbreaking dissipation occurs because of interaction with ocean turbulence. According to this theory, the dissipation creates additional turbulence in the water, and so the energy and momentum goes to the ocean, not the atmosphere.

The presence of following long waves can dampen shorter wind waves. This effect was observed by both laboratory studies with mechanically generated waves (Phillips and Banner 1974; Donelan 1987) and field measurements (Donelan et al. 1997; Drennan et al. 1999; García-Nava et al. 2009, 2012). However, there is ambiguity: does this alleged enhanced attenuation of shorter waves by long waves imply an enhancement of energy and momentum to the atmosphere or to the ocean? If the shorter waves are induced to break more often due to the modulation or ''concertina effect'' of the long waves, then this flux is clearly to the ocean, and the turbulent kinetic energy flux (TKEF) to the ocean is presumably increased by the swells. On the other hand, if the swells are causing the shorter waves to release more energy and momentum to the atmosphere [an outcome of the Ardhuin et al. (2010) formulation, as will be explained below], the result is very different. This manner of enhanced damping of short waves by swells will result in reduction in the energy, steepness, and breaking of the shorter waves, and as a result TKEF to the ocean is reduced (see details in section 3).

In this study, the TKEF change by Southern Ocean swells using both theories (upward versus downward fluxes via nonbreaking dissipation) will be explored with primary focus on the first (upward) theory since it shows an interesting correlation with ENSO and the IOD. Our results are presented in five sections. The methodology is described in section 2; uniform wind experiments are used to demonstrate the effect of swells on TKEF in section 3; the TKEF change at the Niño-3 region and southeastern Indian Ocean due to Southern Ocean swells are presented in section 4; a discussion section is given in section 5; and finally a summary is given in section 6.

2. Method

The wind-wave model, WAVEWATCH III (WWIII) version 4.18, developed and used operationally at the National Centers for Environmental Prediction (NCEP) (Tolman et al. 2014) is used for this study. WWIII computes the evolution in space and time of the wave spectrum, which for the present study is discretized using 36 directions and 40 intrinsic (relative) frequencies extending from 0.0285 to 1.1726 Hz, with a logarithmic increment of $f(n + 1) = 1.1f(n)$, where $f(n)$ is the nth frequency. The wave model is built on a latitude–longitude grid with a horizontal resolution of 0.5°. The effects of unresolved islands are included in the simulations through subgrid obstacle treatment (Tolman 2003).

In WWIII and other third-generation wave models, the evolution of the wave spectrum $F(\sigma, \theta, \mathbf{x}, t)$ is described by means of the wave action conservation equation

$$\frac{\partial}{\partial t}N + \nabla_x \dot{x}N + \frac{\partial}{\partial k}\dot{k}N + \frac{\partial}{\partial \theta}\dot{\theta}N = \frac{S_{\text{atm}} + S_{\text{nl}} + S_{\text{oc}} + S_{\text{bot}}}{\sigma}, \tag{1}$$

where $N(k, \theta, \mathbf{x}, t) = F(k, \theta, \mathbf{x}, t)/\sigma$ is the wave action spectrum that depends on the angular frequency σ from a frame of reference relative to any local current (zero in this study), wavenumber k, wave direction θ, distance vector $\mathbf{x}$, and time t. On the left-hand side of Eq. (1), $\dot{x} = dx/dt = c_g + U$, $\dot{k} = dk/dt$, and $\dot{\theta} = d\theta/dt$ are the propagation speed of the waves in the $\mathbf{x}$, k, and θ dimensions. The spectral source functions on the right-hand side of Eq. (1) are grouped into their atmospheric S_{atm}, nonlinear scattering S_{nl}, oceanic S_{oc}, and bottom S_{bot} sources. Note that S_{nl} represents all processes that lead to an exchange of wave energy between the different spectral components, whereas S_{oc} is restricted to wave breaking and wave turbulence interaction.

a. AET10 parameterization

The WAMF and momentum flux reduction due to the damping of short wind waves by swells are calculated as a swell dissipation term in WWIII (Ardhuin et al. 2010, hereafter AET10), and thus as a negative contribution of energy to the total source term.

The atmospheric source, S_{atm} gives the flux of energy from the atmospheric nonwave motion to the wave motion. It is the sum of a wave generation term S_{in} and a wind generation term S_{out}. The latter is often referred to as negative wind input, which is primarily intended as a swell dissipation term, although it should be kept in mind that the term acts on all frequencies, not just swell frequencies, and so it is more properly referred to as a negative wind input, an wave-to-atmosphere energy flux, or a nonbreaking dissipation source function. This is an energy sink, that is, a negative contribution to the total source term in AET10:

$$S_{\text{out}}(k,\theta) = -C_{\text{dsv}}\frac{\rho_a}{\rho_w}(2k\sqrt{2\nu_a\sigma})F(k,\theta), \quad \text{Re} < \text{Re}_c \quad \text{and} \tag{2}$$

$$S_{\text{out}}(k,\theta) = -\frac{\rho_a}{\rho_w}(16 f_e \sigma^2 u_{\text{orb}}/g)F(k,\theta), \quad \text{Re} \geq \text{Re}_c, \tag{3}$$

where g is gravity. The boundary Reynolds number is defined as

$$\text{Re} = 4u_{\text{orb}}a_{\text{orb}}/\nu_a, \tag{4}$$

where u_{orb} and a_{orb} are the significant surface orbital velocity and displacement amplitude, and ν_a is the air viscosity set to be $1.4 \times 10^{-5}\,\text{m}^2\,\text{s}^{-1}$ in our experiment. The critical Reynolds number Re_c is set to be 2×10^5 following AET10. In the equations, k is the wavenumber, ρ_a and ρ_w are the air and water density, C_{dsv} is a constant set to be 1.2 following AET10, and f_e is a function of the friction velocity u_*, u_{orb}, and the angle difference between wave and wind $(\theta - \theta_u)$:

$$f_e = s_1\left\{f_{e,\text{GM}} + [|s_3| + s_2\cos(\theta - \theta_u)]\frac{u_*}{u_{\text{orb}}}\right\}, \tag{5}$$

in which $f_{e,\text{GM}}$, s_1, s_2, and s_3 are constants set to be 0.003, 0.8, −0.018, and 0.015 as suggested by AET10.

The presence of swells will increase u_{orb}, and hence energy and momentum losses to the atmosphere (S_{out}) for all spectral components. This slightly reduces the energy of wind sea, which via the highly nonlinear dissipation term of AET10 results in significantly reduced breaking of short waves in the prognostic spectrum. Since wave breaking injects turbulence (TKEF) in the upper layers of the ocean (Cavaleri et al. 2012), the swells cause a small, indirect reduction of this TKEF.

The TKEF from wave to the ocean is calculated in WWIII as the difference between initial energy E_{initial} and final energy E_{final}, plus S_{atm} and S_{nl}, and minus the energy lost to the bottom boundary layer S_{bot}, based on Eq. (1) above:

$$\text{TKEF} = (E_{\text{initial}} - E_{\text{final}})/\Delta t + S_{\text{atm}} + S_{\text{nl}} - S_{\text{bot}}, \tag{6}$$

where Δt is the source term time step; by convention, positive TKEF implies a flux from waves to ocean and positive S_{atm} implies a flux from atmosphere to waves. This can be explained by considered a simple case where a grid cell contains wind sea in balance with the local wind (in steady state) and then introducing swell. This introduction results in a negative contribution to S_{atm} at both swell and wind-sea frequencies: S_{atm} remains positive but is reduced. As a result, TKEF as computed using Eq. (6) is reduced.

The comparison of u_{orb} in the Niño regions indicates an increase of 4%–8% due to Southern Ocean swells (Fig. 1), which is one important contribution for TKEF reduction in that region. It will be shown in section 3 below that the wind-sea damping plays a dominant role on TKEF reduction, and thus is the focus for this study.

b. ZET15 parameterization

In contrast to the assumption that swell energy is transferred to the atmosphere and attenuates the TKEF into the ocean, the theory by Babanin (2006) argues that the swell attenuation is due to the interaction with ocean

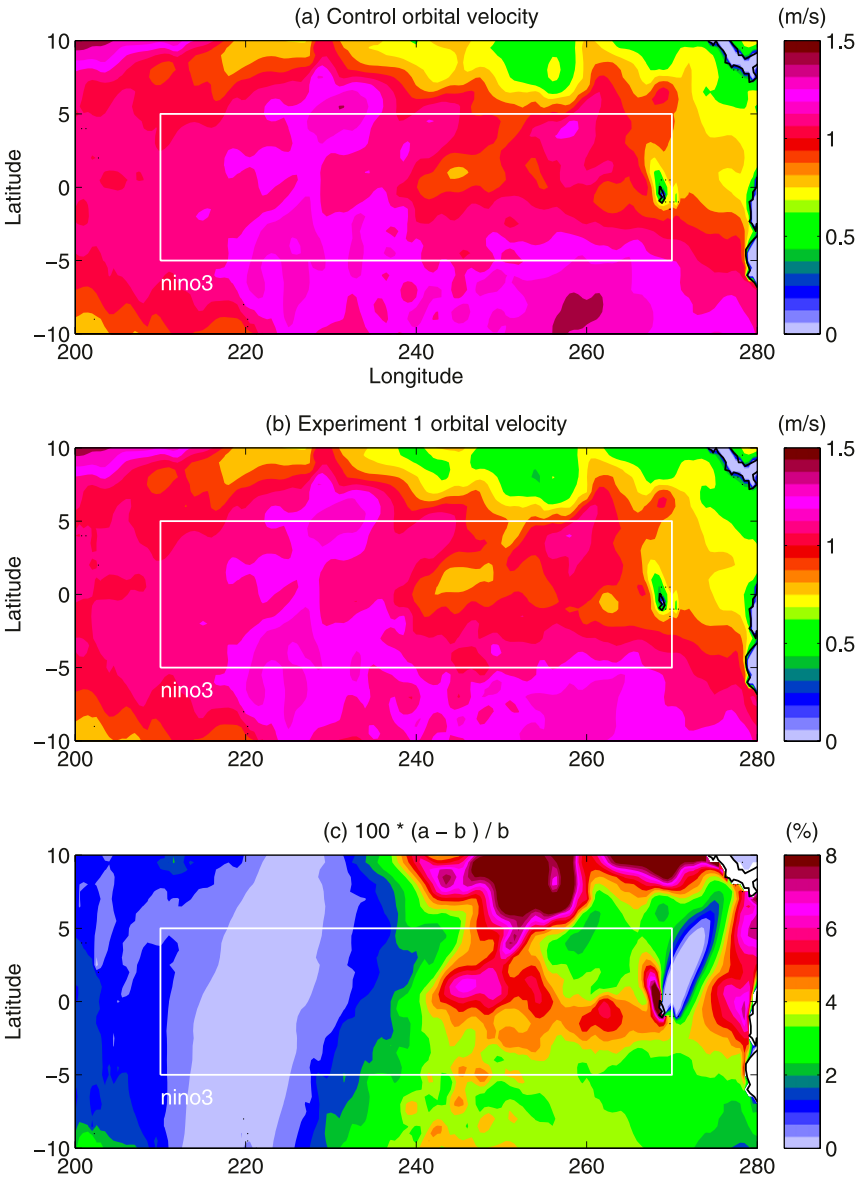

FIG. 1. Significant orbital velocity at 1200 UTC 4 Aug 2006 for the (a) control experiment and (b) experiment 1. (c) The u_{orb} increase due to Southern Ocean swells [100%(control − experiment 1)/experiment 1]. The white box gives the location of the Niño-3 region.

turbulence, and thus swells will transfer energy into the ocean when they dissipate, in the form of additional turbulence. Zieger et al. (2015, hereafter ZET15) parameterized this effect in WWIII as the ''swell dissipation'' $S_{\mathrm{swl}}(k, \theta)$, which is added to the dissipation term S_{oc} in Eq. (1). Like the AET10 swell dissipation, this formulation acts on all frequencies, not just swells, and is more correctly referred to as a nonbreaking dissipation source function:

$$S_{\mathrm{swl}}(k,\theta) = -\frac{2}{3} b_1 \sqrt{B_n(k)} F(k,\theta). \tag{7}$$

The spectral saturation is defined as

$$\sqrt{B_n(k)} = A(k) N(k) \sigma k^3 \tag{8}$$

and the inverse of the directional spectral narrowness is calculated as

$$A^{-1}(k) = \int_0^{2\pi} [N(k,\theta)/N_{\max}(k)]\, d\theta, \tag{9}$$

with $N_{\max}(k) = \max\{N(k, \theta)\}$. Note that b_1 in Eq. (7) is a nondimensional coefficient, which Young et al.

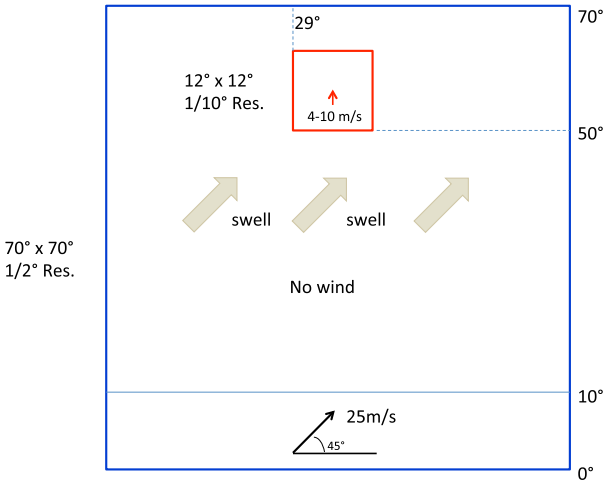

FIG. 2. Model domain setup for the uniform wind experiment. The outer domain (blue box) is 70° by 70° in latitude/longitude with 0.5° resolution; a 25 m s^{-1} northeast wind is applied south of 10° with no winds north of it. The inner domain is 12° by 12° in latitude/longitude with 0.1° resolution, and uniform northward winds of 4–10 m s^{-1} are applied for the whole domain.

(2013) estimated to fall between 2×10^{-4} and 14×10^{-4}. For this study $b_1 = 2.5 \times 10^{-4}$ is used following ZET15.

Like AET10, this parameterization is applied to the entire wave spectrum. However, unlike the AET10 parameterization, it will be shown in section 3 below that the increase in TKEF caused by the presence of swell is (in this formulation) occurring almost entirely in the swell part of the spectrum. In fact, it is evident from the equations that dissipation is strictly local in frequency space, meaning that the presence of swell cannot directly affect the source function at higher frequencies. However, since there may be indirect effects via other source functions, numerical computations are performed below. It is also noteworthy, that unlike AET10, there is no dependence on the local wind (i.e., the friction velocity in this parameterization).

3. Swell effect on TKEF

We use a uniform wind experiment to demonstrate the calculation of TKEF. Two nested domains are used for this calculation (Fig. 2). The outer domain is set up to be 70° by 70° in latitude and longitude direction with 0.5° resolution. The inner domain is placed inside the northern part of the outer domain 50° from the southern boundary and 29° from both the western and eastern boundary. It is set up to be 12° by 12° in latitude and longitude with 0.1° resolution.

To create swell for boundary conditions, a uniform 25 m s^{-1} wind blowing toward the northeast is applied south of 10° in the outer domain with no winds north of 10° to mimic swells generated from the Southern Ocean. WWIII is run for 5 days on this domain. The boundary conditions around the inner domain are saved at the end of the 5-day calculation (Fig. 3) and used as constant boundary forcing for the inner domain. Two sets of experiments are conducted in the inner domain with uniform wind blowing northward for both the AET10 and ZET15 parameterizations. In experiment set one, WWIII is run on the inner domain without swell boundary conditions applied; in experiment set two, WWIII is run on the inner domain with swell boundary conditions from the outer domain. The difference between these two experiments will give the TKEF change due to the presence of remote swells. For each set of experiments, six runs with uniform northward winds range from 5 to 10 m s^{-1} at 1 m s^{-1} increments are conducted. The choices of winds are based on seasonal means in the Niño-3 region (see the appendix). All experiments are run for 2 days until the waves in the domain reach steady state.

a. AET10 parameterization

The TKEF from the AET10 parameterization are plotted in Fig. 3 at the center of the domain for the two sets of experiments. We can see that the TKEF increases with wind speed with and without remote swells. The reduction of TKEF by remote swells in general increases with wind speed. This ratio will also vary when the magnitude of remote swell changes.

To understand the relative importance of the nonbreaking dissipation source functions on TKEF reduction, we decompose the terms on the right-hand side of Eq. (6) (Figs. 3e,f) for both set of experiments. These experiments are conducted in deep water (4000 m), so $S_{\text{bot}} = 0$. Theoretically, the nonlinear interaction term (S_{nl}) should integrate to zero as well. The value of S_{nl} is not exactly zero in the model because of numerical errors and/or the treatment of the high-frequency tail in the spectrum, but are negligible compared to other terms. Since the results are analyzed at quasi-steady state, the $(E_{\text{init}} - E_{\text{final}})/\Delta t$ term is also very small and negligible (Fig. 3f). So, this leaves us the negative source term S_{atm} only (Fig. 3e). With the presence of remote swells, we can clearly see the reduction of the wind sea part of S_{atm}, while the swell contribution to the S_{atm} is so small we can hardly see the difference between the two sets of experiment. Thus, the reduction of TKEF is caused by damping of wind sea (and therefore reduced breaking of wind seas) by the wave-to-atmosphere source function, which is enhanced by swells via u_{orb}. The contribution to TKEF

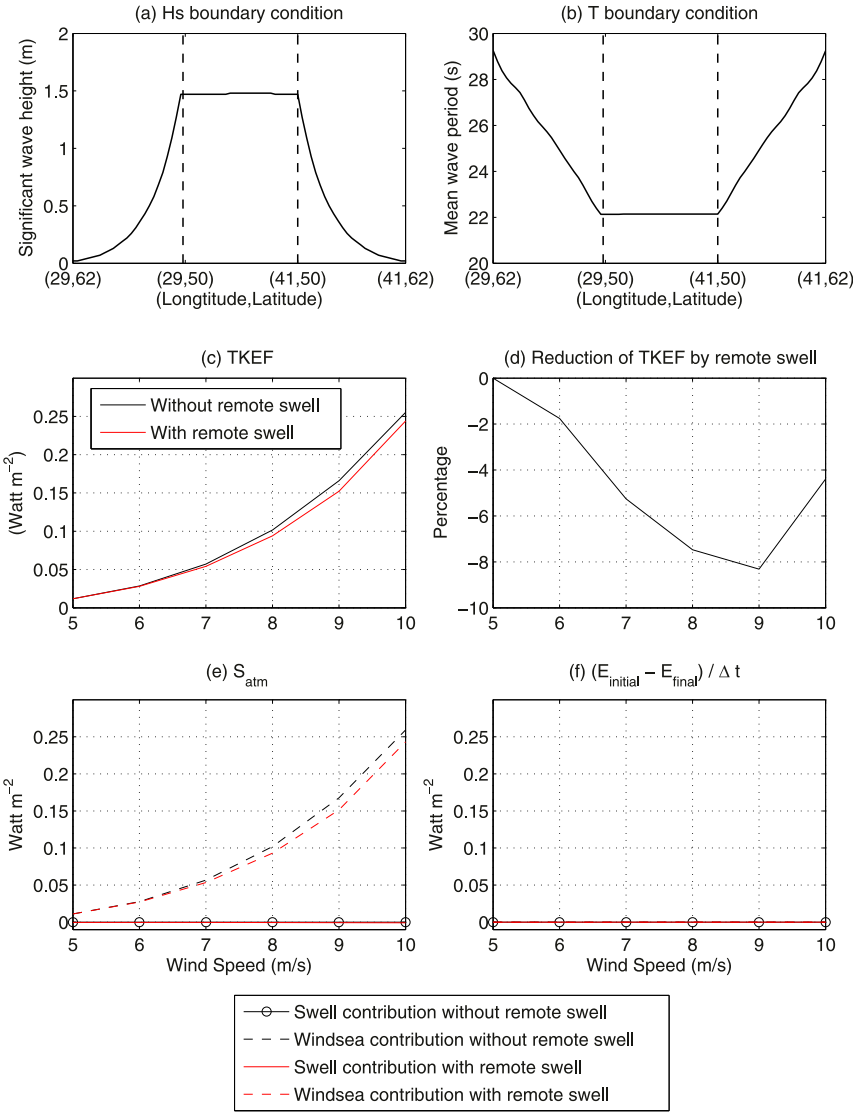

FIG. 3. (a) Significant wave height and (b) mean wave period along the western (from 29° lon, 62° lat to 29° lon, 50° lat), southern (from 29° lon, 50° lat to 41° lon, 50° lat), and eastern (from 41° lon, 50° lat to 41° lon, 60° lat) boundary of the inner domain at the beginning of the simulation. They do not change during the 2-day simulation period. (c) TKEF with (red) and without (black) remote swells; (d) the percentage of TKEF reduction by remote swells; (e) swell (solid) and wind sea (dashed) contribution to S_{atm} with (red) and without (black) remote swells; and (f) swell (solid) and wind sea (dashed) contribution to wave energy change rate with (red) and without (black) remote swells.

change from dissipation at swell frequencies is negligible: this is expected, since swells are not breaking: TKEF is zero at the swell frequencies with or without swells.

b. *ZET15 parameterization*

Since the ZET15 parameterization is applied to S_{oc} term in WWIII, this source term is compared in Fig. 4 at the center of inner domain. We see that, for the cases with and without remote swells, the S_{oc} term is almost identical at high frequencies. A sharp peak is observed at the low frequencies for the cases with remote swells, indicating that the change in TKEF caused by swells is associated with nonbreaking dissipation source term at the swell frequencies. As expected, the nonbreaking dissipation term is active at the wind-sea frequencies, but is not affected by the presence of swell. Also the dissipation at swell frequencies is the same for different

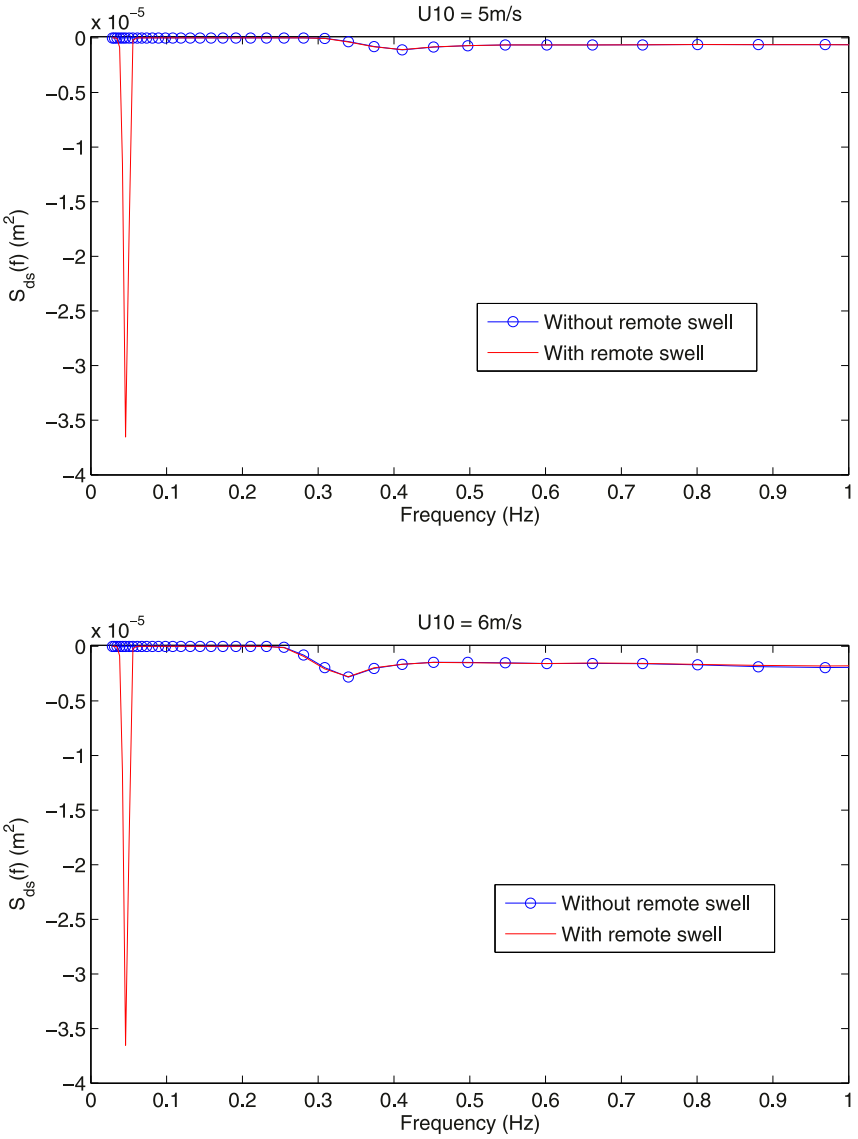

FIG. 4. Dissipation source spectrum with (red) and without (blue) remote swells for (top) 5 and (bottom) 6 m s^{-1} winds.

wind speeds because this parameterization is not affected by the local winds.

4. TKEF change in the Niño-3 region and southeastern Indian Ocean

In this section, the effects of midlatitude swells on TKEF to the ocean are analyzed. Four sets of experiments are conducted using WWIII, with specific swell sources omitted in some experiments in order to quantify their relative importance. This approach loosely resembles the censoring of generation zones in a global wave model done by Alves (2006) for studying contributions of swells to the global wave climate. In the control experiment, the wave field is simulated for the whole globe. In experiment 1, artificial land is placed south of 39°S to block swells from the Southern Ocean. In experiment 2, artificial land is placed north of 39°N to block the swells from the Northern Hemisphere midlatitude storm region. Finally, in experiment 3, artificial land is placed both south of 39°S and north of 39°N to eliminate the swells from all midlatitude storms.

WWIII is run continuously, starting from calm seas, for 14 years from 1 January 1997 to 31 December 2010 for all experiments using both the AET10 and the ZET15 parameterizations separately. Hourly winds and daily sea ice coverage are obtained from the NCEP Climate Forecast System Reanalysis (Saha et al. 2010)

to force the model. The results are saved at 6-h intervals. Since the model spinup time is dominated by the transit times of swell through the Pacific Ocean (less than a month), the results are analyzed from 1 May 1997 to 31 December 2010. Both El Niño and La Niña events occurred during these 14 years including one strong El Niño in 1997 and two strong La Niña years in 1999 and 2010. Most interestingly, 2006–08 are three consecutive positive IOD year events. Such an occurrence is very rare. In particular, the 2007 positive IOD occurred in a La Niña year, which generally is unfavorable for the development of IOD events (Cai et al. 2009).

The results from the AET10 parameterization are analyzed in detail first since they present an interesting correlation with ENSO and IOD. Results from ZET15 parameterization are then given and discussed at the end. The 6-hourly WAMF and TKEF reduction to the ocean are averaged to produce the seasonal means defined as follows: December–February (DJF), March–May (MAM), June–August (JJA), and September–November (SON).

a. Pacific Ocean using AET10

1) WAMF AND TKEF REDUCTION

The seasonal mean WAMF for the 14-yr period in the tropical Pacific and Indian Ocean from the control experiment is presented in Fig. 5. The Niño-3 region is given on the figures for reference. Notice that the magnitude of WAMF is higher to the north and south of the Niño-3 region and decreases gradually toward the equator for all seasons. The WAMF values in the Niño-3 region reach their annual maximum during the austral winter (JJA) when the Southern Ocean swells are the strongest, and become almost zero during the austral autumn–boreal spring (MAM) when both the Southern Ocean and North Pacific swells are weak. It is interesting to notice that the WAMF values in the Niño-3 region are also very small during the boreal winter (DJF) when the swells from the North Pacific midlatitude storm region are the strongest. This is because, for all four seasons, the Southern Ocean swells are mainly propagating northeast toward the equatorial eastern Pacific and contribute significantly to the swell energy in the Niño regions (not shown). The swells emitted from the North Pacific midlatitude storm region, on the other hand, are mainly propagating southeast toward the west coast of North America. Only a very small fraction of the swell energy from the north can reach the Niño regions (not shown), even during the boreal winter (DJF) when the swells are the strongest. Thus, the WAMF is dominated by Southern Ocean swells in the Niño-3 region while swells from the North Pacific hardly play any role.

Furthermore, the El Niño/La Niña phenomenon is most affected by SST anomalies during the JJA and SON seasons. Consequently, we limit our analysis to the tropical Pacific WAMF and TKEF changes by midlatitude swells during JJA and SON in this study.

The percentage of WAMF and TKEF reduction due to Southern Ocean swells [(control − experiment 1)/control] are first analyzed in 2006 (Fig. 6) since it is an El Niño year with positive IOD. A tongue-shaped, well-defined area is found in the eastern half of the Niño-3 region with more than 60% increase of WAMF by Southern Ocean swells near its eastern boundary for both seasons. In general, the contribution is stronger during JJA when the Southern Ocean swells are the strongest. The effect in the western part of the Niño-3 region is negligible since less swell energy can reach there due to the sheltering effect by Australia and several island chains in the southwestern Pacific. There is also large WAMF contribution from Southern Ocean swells (up to 60% during SON) in the Indian Ocean. This phenomenon and its possible connection with IOD will be discussed in section 4b.

The TKEF into the ocean is reduced by 3%–4% in the Niño-3 region for both seasons (Figs. 6c,d), but the affected areas are much larger when compared to WAMF. Since the TKEF reduction is not a large number, it is useful to explore whether this effect can be ignored. Thus, the maximum TKEF reduction percentage and the percentage of TKEF reduction exceeding 5% at each grid point are calculated using the 6-hourly model output in 2006 for both seasons in the tropical eastern Pacific (Fig. 7). During JJA, the TKEF reduction can reach 40%–50% in some areas in the eastern part of the Niño-3 region and the TKEF reduction exceeds 5% for about one-fourth of the season. During SON, the maximum TKEF reduction is lower. Since more than 5% of TKEF reduction persists for a considerable period of time during both seasons with maximum reduction up to 50%, its cumulative effect is not negligible, according to the AET10 model.

The same experiments are conducted when Northern Hemisphere midlatitude swells are eliminated (experiment 2) and when midlatitude swells from both Hemispheres are eliminated (experiment 3). It is found that only a small portion of the Northern Hemisphere midlatitude swells can reach the tropics, thus having minimal impact on the WAMF and TKEF. The analysis also shows that the effect of midlatitude swells on WAMF and TKEF from both hemispheres can be linearly added in the system globally.

2) TKEF REDUCTION AND SST ANOMALIES IN EL NIÑO REGIONS

Next, the correlation between the AET10 TKEF reduction due to Southern Ocean swells and SST

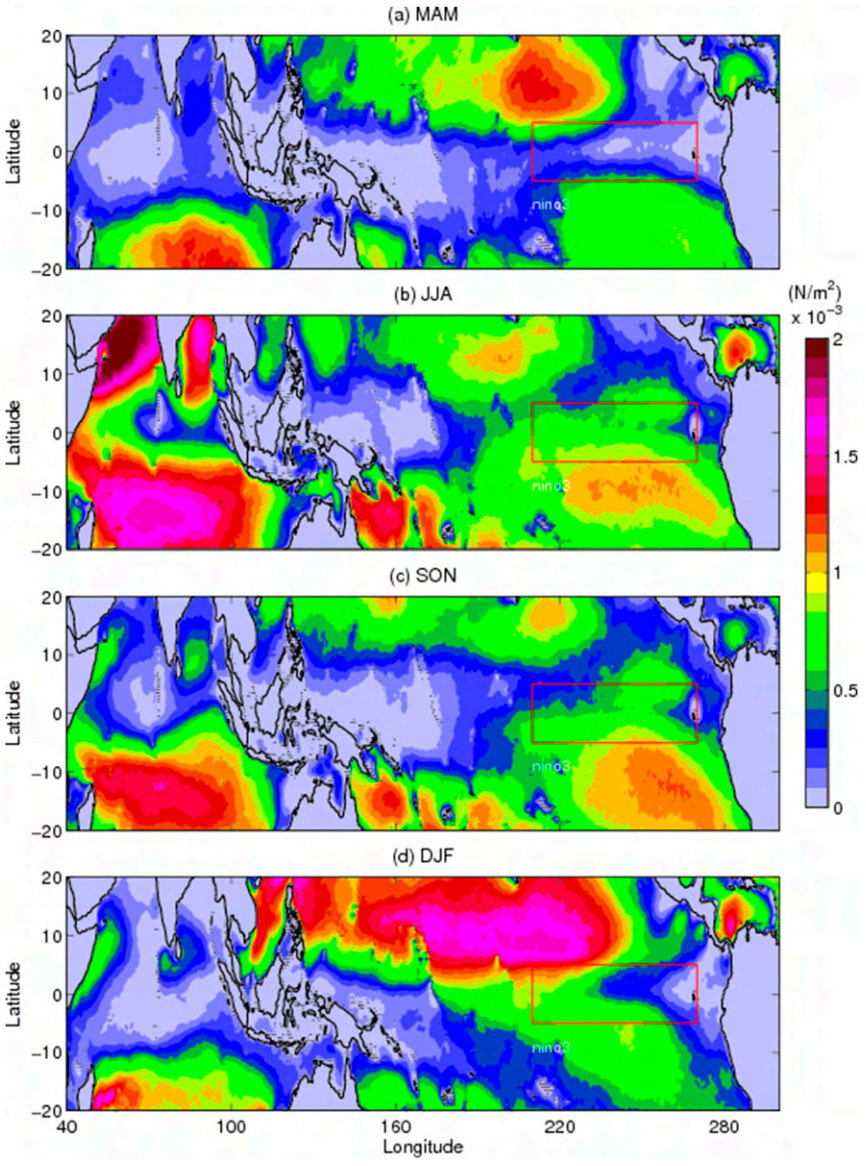

FIG. 5. The 14-yr seasonal mean WAMF in the equatorial Pacific and Indian Ocean during (a) MAM, (b) JJA (c) SON, and (d) DJF. The red boxes give the location of the Niño-3 region.

anomalies in the El Niño regions is calculated. Since the eastern Pacific cold tongue results from diapycnal upwelling through all layers of the Equatorial Undercurrent (Wyrtki 1981; Sloyan et al. 2003), we calculate the mean TKEF reduction along the equator between 230° and 270°E for both seasons and compare its anomaly (average value for entire calculation period removed) with the SST anomaly in the Niño-3 region from 1997 to 2010 (Fig. 8). The SST anomalies are obtained from the National Oceanic and Atmospheric Administration/National Weather Service/Climate Prediction Center (http://www.cpc.ncep.noaa.gov/data/indices/ersst3b.nino.mth.81-10.ascii).

It is interesting to see that the modeled TKEF reduction anomaly is in opposite phase with the SST anomaly. When there is less (more) TKEF reduction—that is, a positive (negative) anomaly—from Southern Ocean swells, the SST becomes colder (warmer) in the region. Since, according to AET10, the Southern Ocean swells inhibit turbulent mixing, a positive TKEF reduction anomaly (less TKEF reduction), as was the case in 2007, a La Niña year, means less inhibition (Figs. 8g,h) and thus higher turbulent mixing in the water column that may lead to more surface cooling. In the El Niño year of 2006 the opposite anomalies were seen, namely a negative TKEF reduction anomaly

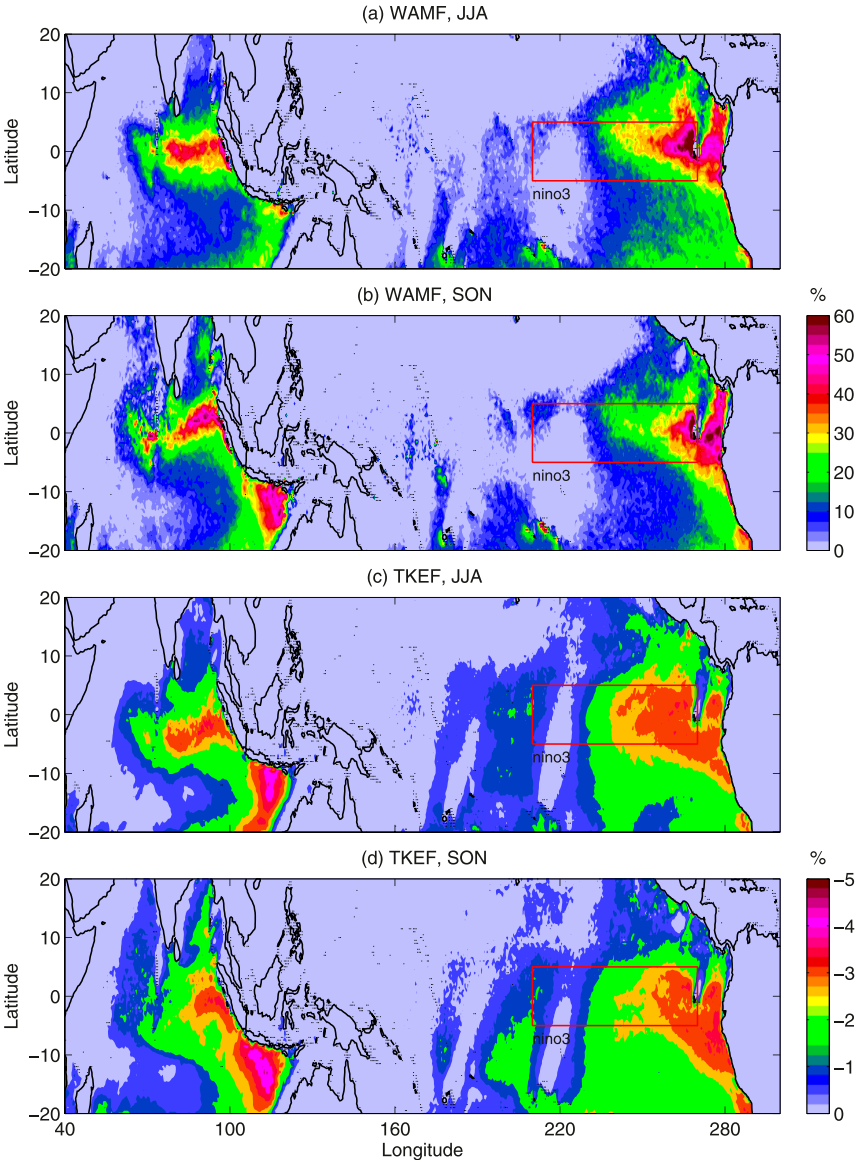

FIG. 6. Percentage change of seasonal mean WAMF due to Southern Ocean swells [100%(control − experiment 1)/control] during (a) JJA and (b) SON 2006, and percentage change of seasonal mean TKEF due to Southern Ocean swells [100%(control − experiment 1)/control] during (c) JJA and (d) SON 2006.

(more TKEF reduction) and reduced turbulent mixing and higher SST (Figs. 8e,f). One exception to this calculation is the JJA seasons in 2000 and 2001, which show a weak negative TKEF reduction anomaly while the SST anomaly is also negative. One possible reason could be that since 1999 is a strong La Niña year with a large cold SST anomaly and deeper than usual mixed layer depth, the relatively weak negative TKEF reduction and/or decrease in turbulent mixing induced by the Southern Ocean swells is not sufficiently strong to significantly impact the cold SST anomaly. Further research needs to be conducted to better understand this phenomenon.

b. *Indian Ocean using AET10*

Saji et al. (1999) and Webster et al. (1999) found a SST dipole mode in the tropical Indian Ocean, which accounts for about 12% of the SST variability in the Indian Ocean and, in its active years, also causes severe rainfall in eastern Africa and droughts in Indonesia. To compare with their study, the TKEF reduction due to Southern Ocean swells is calculated for the same bimonthly

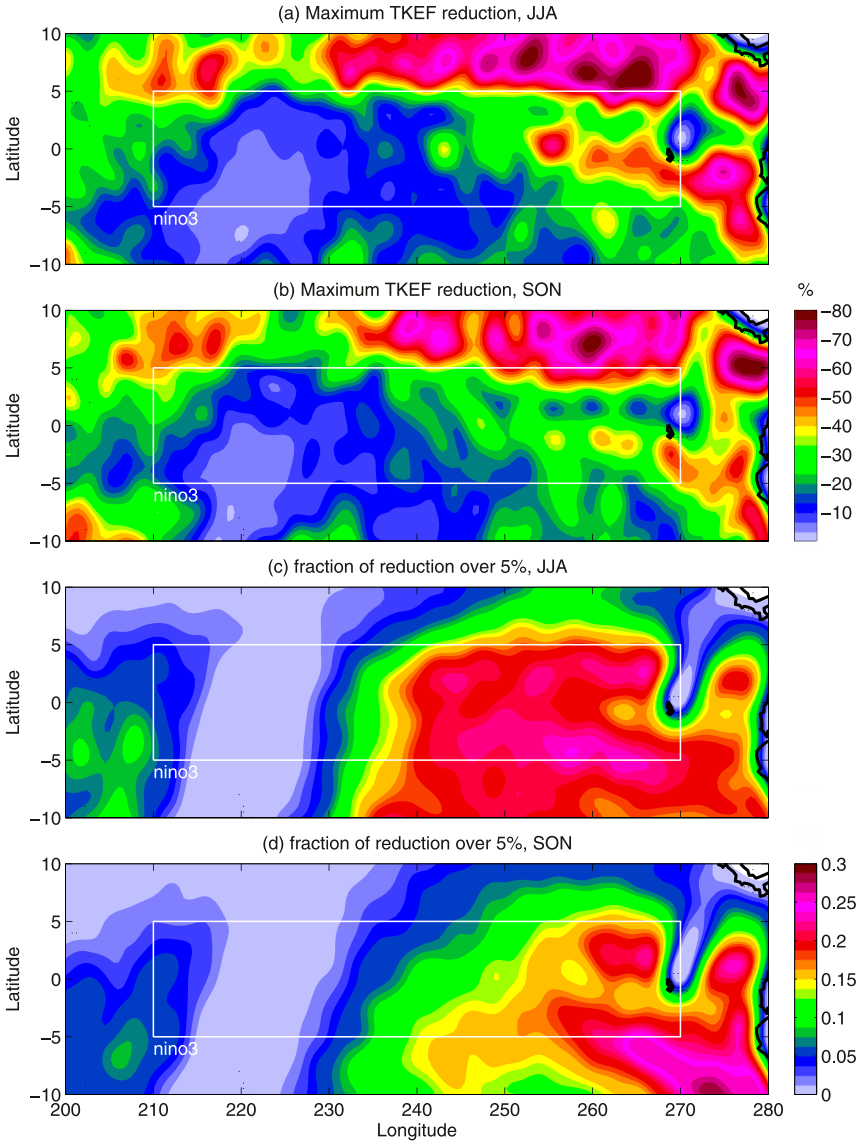

FIG. 7. Maximum TKEF change due to Southern Ocean swells in the Niño-3 region [100%(control − experiment 1)/control] during (a) JJA and (b) SON 2006, and fraction of more than 5% TKEF reduction by Southern Ocean swells during (c) JJA and (d) SON 2006.

averages in 2006 (Fig. 9a1–a4). TKEF reduction (by ~3% of the total TKEF) appears in the Lombok Strait region by May–June. The reduction increases in July–August (by ~5% of the total TKEF) and the affected area extended equatorward along the coast of Sumatra. In September–October, the magnitude of model TKEF reduction slightly weakens with further extension toward the equator while the TKEF reduction in the area south of the coast of Java starts to retreat southward. Finally, the TKEF reduction rapidly weakens in November–December. This is very well correlated with the SST behavior in Saji et al. (1999), where they found the cool SST anomalies first appear in the vicinity of the Lombok Strait by May–June, intensify and migrate toward the equator along the Indonesian coastline in July–August, peak in September–October, and then rapidly diminish in November–December.

According to our wave model results, the Southern Ocean swells inhibit TKEF to the ocean, which implies that the turbulent mixing in the oceanic mixed layer will be reduced. This reduction may work in a positive way to help maintain a colder surface layer in this region when the SST cools due the increased evaporation caused by the southeasterlies in the eastern Indian Ocean (Behera and Yamagata 2001). More

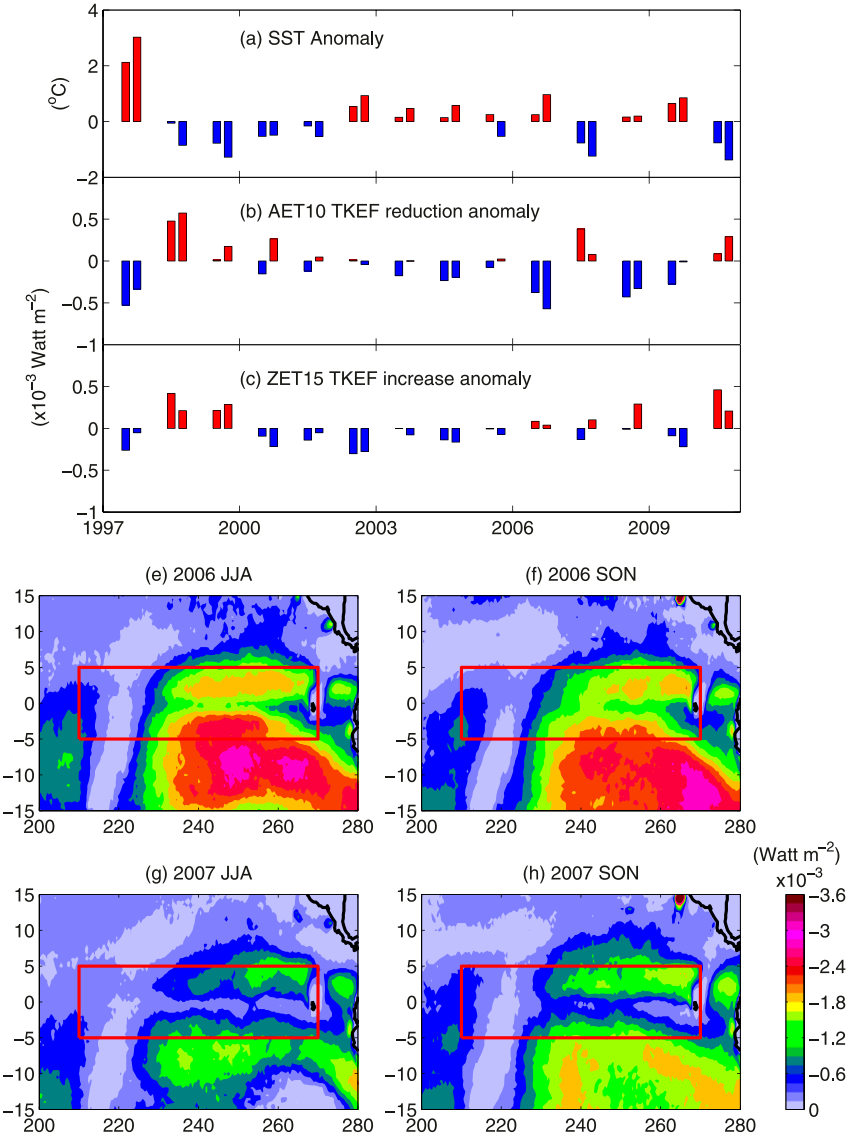

FIG. 8. (a) Climate Prediction Center SST anomalies; (b) mean TKEF reduction anomaly (average value for entire calculation period removed) using AET10; and (c) mean TKEF increase anomaly (average value for entire calculation period removed) using ZET15 in the Niño-3 region during JJA and SON season. Also shown are TKEF changes (control − experiment 1) due to Southern Ocean swells during (e) JJA and (f) SON 2006 and (g) JJA and (h) SON 2007.

discussions on the possible physical process are given in section 5.

To further diagnose this, we analyze the TKEF reduction magnitude from 1997 to 2009. During the continuous three years of positive IOD from 2006 to 2008, the TKEF reduction patterns in 2007 and 2008 are very similar to 2006 with some differences in May–June 2007 (Fig. 9b1). The TKEF reduction not only appears in the Lombok Strait region but is extended to the central Indian Ocean. Thus, the turbulent mixing in the water column is reduced by the Southern Ocean swells not only in the Lombok Strait, but also in the central Indian Ocean during these two months in 2007.

A similar pattern and magnitude of TKEF reduction is also observed in 1997, which is another positive IOD year. During the non-IOD years (1998–2005 and 2009), the TKEF reduction are much smaller in general. Examples of these non-IOD years are given in Fig. 10 for 1998 (after positive IOD year 1997), 2000, and 2005 (before positive IOD year 2006).

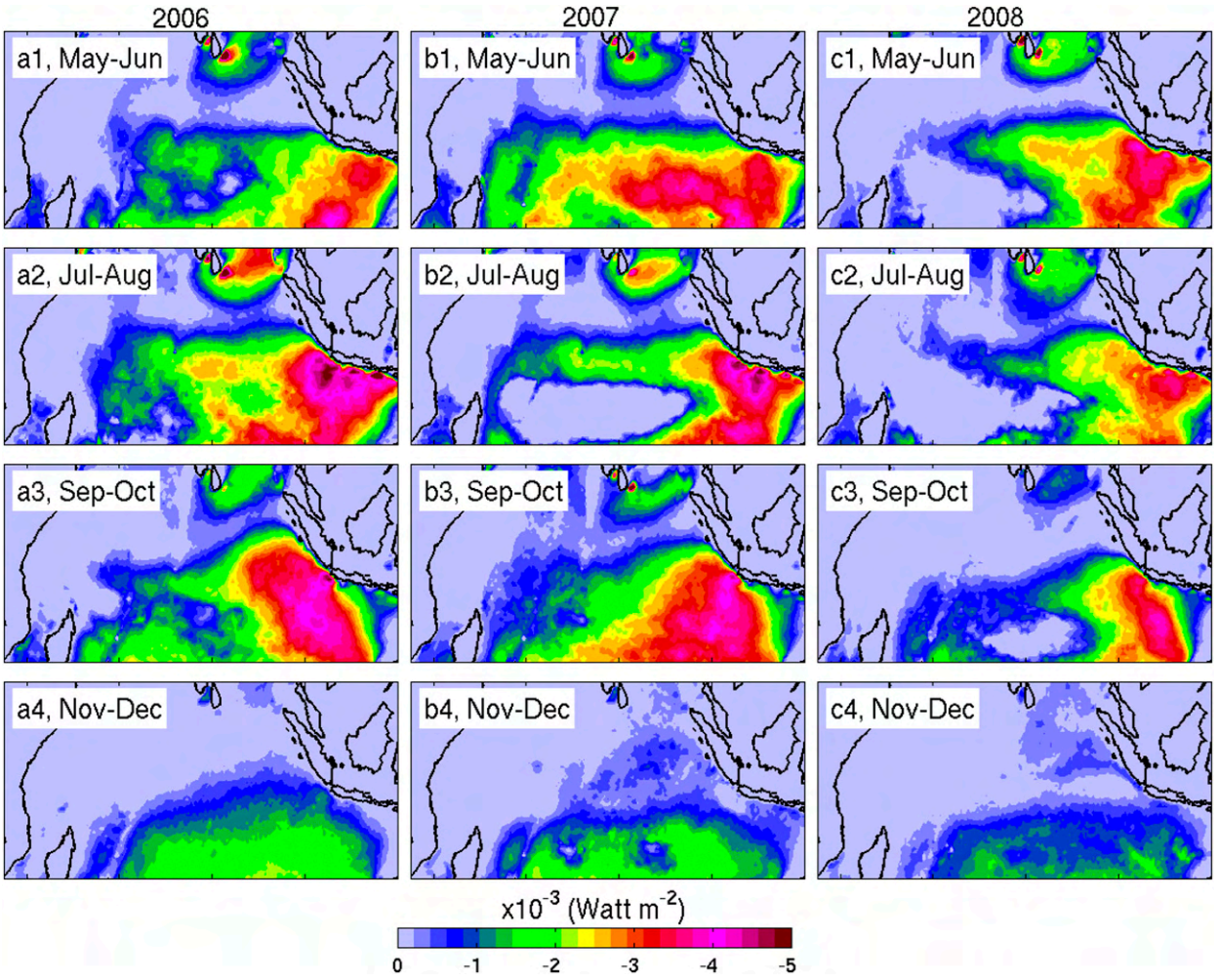

FIG. 9. (left) Bimonthly averaged TKEF change due to Southern Ocean swells (control − experiment 1) during (a1) May–June, (a2) July–August, (a3) September–October, and (a4) November–December in 2006. (center), (right) As at left, but for 2007 and 2008, respectively.

c. *Model results using ZET15*

The ZET15 parameterization, in contrast, shows stronger effects on TKEF with up to 6% increases in the Niño-3 region and more than 6% in the IOD regions (not shown). However, the anomalies of TKEF increase (same calculation as described for the TKEF reduction anomalies above) do not show any correlation with the SST anomalies in either the Niño-3 region (Fig. 8) or the Indian Ocean (not shown). This is more likely because within the ZET15 nonbreaking dissipation parameterization, the swells have no effect on the wind sea, while the AET10 parameterization does produce this effect. These results suggest that the swell dissipation itself is not correlated with ENSO and IOD, whether it goes up to the atmosphere or down into the ocean. Rather, it is the AET10 parameterization's TKEF reduction due to the damping of short wind waves by swells that is correlated with the ENSO and IOD.

5. Discussion

In section 4a, an interesting anticorrelation is found between the AET10 TKEF reduction anomaly and SST anomaly in the Niño-3 region. An important question is whether this correlation is just a consequence of a correlation between Southern Ocean swells and ENSO, although the fact that no correlation was found for the ZET15 scheme suggests that is not the case. To answer this question, we analyze the correlation between Southern Ocean swells and the Southern Ocean Oscillation index (SOI).

The 29-yr (1981–2009) atmosphere and wave climatology produced by Fan et al. (2012) using a coupled

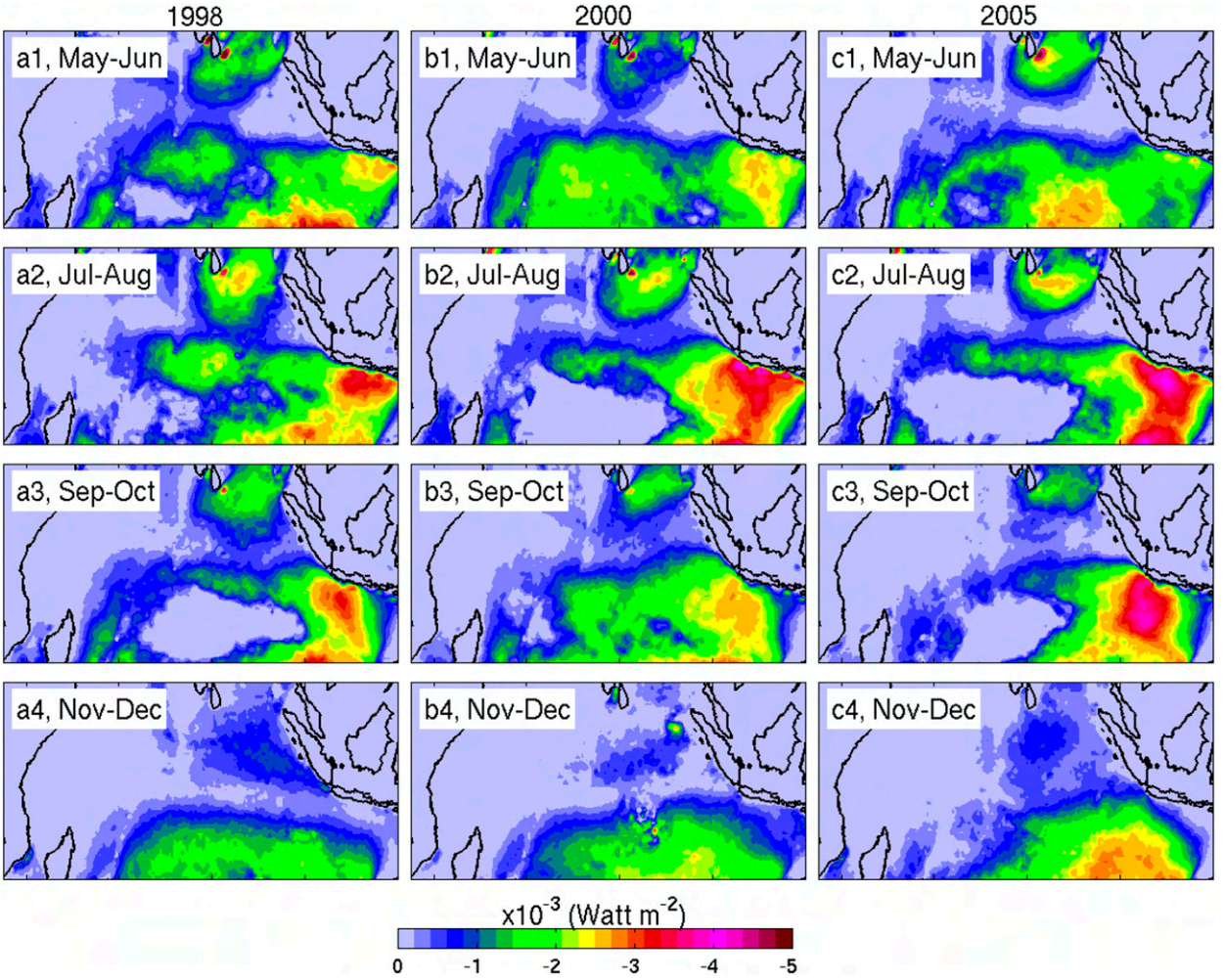

FIG. 10. (left) Bimonthly averaged TKEF change due to Southern Ocean swells (control − experiment 1) during (a1) May–June, (a2) July–August, (a3) September–October, and (a4) November–December in 1998. (center), (right) As at left, but for 2000 and 2005, respectively.

atmosphere–wave model is used for this purpose. The SOI for the coupled model is derived using the standardized anomaly of the mean sea level pressure difference between Tahiti and Darwin following Fan et al. (2012). Correlations between monthly mean swell energy, swell period, and the SOI are calculated at lags ranging from −12 to 12 months with 1-month intervals. Weak correlations with the SOI are found for both swell energy and period in the Niño-3 region with the SOI leading the swell energy and period by 3–10 months. The correlations with 3-, 6-, and 10-month lag are presented in Fig. 11.

As Rasmusson and Carpenter (1982) have pointed out, the first development of SST anomalies occurs off the South American coast several months before the SOI responds to equatorial SST anomalies. Southern Ocean swells will reach the Niño-3 region within a couple of weeks, so the observed correlation is not likely to be a direct response to ENSO-related wind changes over the Southern Ocean.

The relationship between zonal wind stress and SST anomalies in the Niño-3 region has been known since the 1960s (e.g., Ichiye and Petersen 1963; Bjerknes 1966; see also Philander 1990), and since the TKEF reduction in AET10 is weakly dependent on the friction velocity for high Reynolds numbers, this may be a likely explanation for the correlation found here. An alternative hypothesis is more interesting and proceeds as follows. Wind changes in the Southern Ocean not directly related to the Southern Oscillation may affect the SST anomalies in the Niño-3 region. The swells affect TKEF and hence decrease the turbulent mixing in the oceanic boundary layer. This contributes, although likely in a very limited way, to changes in the ocean dynamics that alter

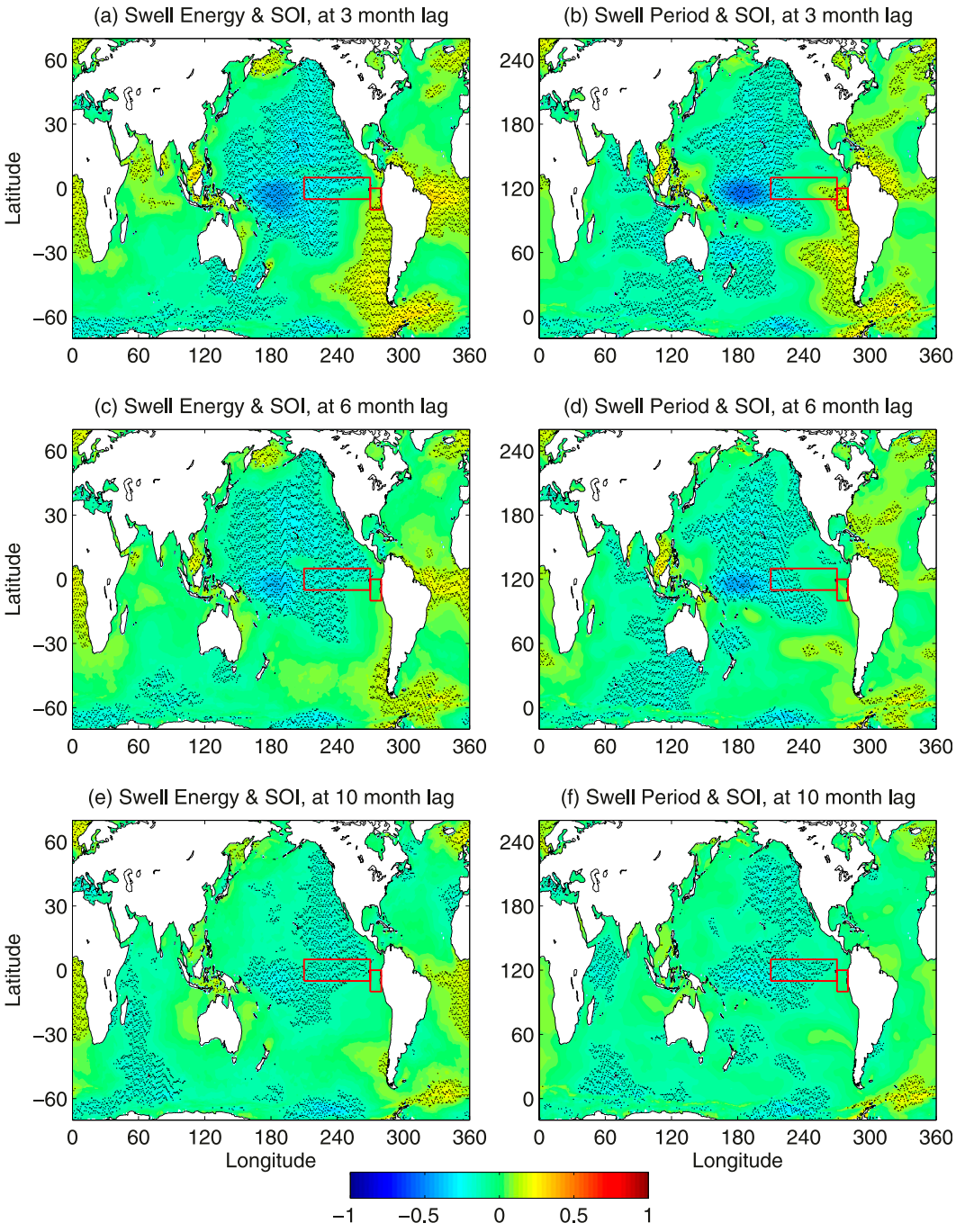

FIG. 11. Correlation between swell energy and SOI at (a) 3-, (c) 6-, and (e) 10-month lag. Correlation between swell period and SOI at (b) 3-, (d) 6-, and (f) 10-month lag. The black dots indicate areas with 95% confidence level.

SST, changing the atmospheric heating; the changes in atmospheric convection result in changes in surface wind and the Southern Oscillation, which in turn alter the swells. The swells clearly only play a minor role in that feedback loop compared to changes in equatorial wind stress and latent and solar heat fluxes, but the cumulative effect of TKEF reduction for the persistent swells could contribute to maintain and enhance an El Niño or La Niña event given the sign of the correlation, and the fact that vertical mixing is a highly nonlinear process with thresholds that determines whether mixing events will occur. Coupled atmosphere–wave–ocean climate model simulations are needed to further explore and understand this potential feedback mechanism.

The AET10 TKEF reduction is also found to be well correlated with the SST cold anomaly at the Lombok Strait in the southeastern Indian Ocean. Two major processes contribute to the SST cooling in this region. First, strong alongshore winds cause upwelling from the Sumatra thermocline along the Java and Sumatra coast, where the upwelled cold thermocline water is advected westward by the offshore currents (e.g., Murtugudde et al. 2000). Second, the southeasterlies in the eastern Indian Ocean cause surface cooling due to increased evaporation (Behera and Yamagata 2001). When this happens, turbulent mixing will mix the cold surface water with the warmer mixed layer beneath to create a colder and deeper mixed layer. According to our wave model results, the Southern Ocean swells can inhibit TKEF to the ocean and thus reduce the turbulent mixing in the oceanic mixed layer. In the absence of deep convection, this effect will lead to a shallower and colder mixed layer and thus helps the development of the positive IOD mode. During the cooling event, deep convection could also occur, which will tend to make a uniform water column and reduce the SST. Turbulent mixing in the water column can weaken stratification and provide favorable preconditions for the deep convection to occur. The reduction in TKEF will reduce turbulent mixing and thus the effect on weakening the stratification. In both situations, the reduction of TKEF by the Southern Ocean swells can work in a positive way to help maintain a colder SST.

An unusual TKEF reduction in the central Indian Ocean is found during May–June 2007. Note that 2007 is a La Niña year, during which the wind stress anomalies are typically in the opposite direction of those found during El Niño years with larger magnitude in the central Indian Ocean (e.g., Jensen 2007). These conditions are unfavorable for the development of a positive IOD (Cai et al. 2009). However, the reduction of TKEF in the central Indian Ocean due to Southern Ocean swells can reduce the effect of large wind stress anomalies and help to eliminate the unfavorable condition for the development of positive IOD. Again, coupled atmosphere–wave–ocean climate models simulations are needed to further explore and understand the relationship between the TKEF reduction and SST cooling during these positive IOD events.

Although not investigated in this study, it is important to mention that swells could also influence SST through its effect on the atmosphere. In the presence of swells outrunning relatively weak winds, the velocity spectra no longer have universal shapes, so the classical Monin–Obukhov similarity theory is no longer valid (Drennan et al. 1999). The presence of counter- and cross-swells can result in drag coefficients that are much larger than the value for a pure wind sea (Kudryavtsev and Makin 2004; Grachev et al. 2003), while upward momentum transfer is associated with fast-traveling swell running in the same direction as the wind (Makin 2008; Grachev et al. 2003; Grachev and Fairall 2001). Both phenomena are typical in the tropics where counter- and cross-swells dominate the open ocean (Fan et al. 2014). These changes in momentum fluxes will change temperature and humidity profiles and sensible and latent heat fluxes that eventually change SST.

6. Summary

This study analyzes the correlations between the effects of Southern Ocean swells and ENSO/IOD using a numerical modeling approach. Two possible theories on swell dissipation are investigated: in one case, swell energy is lost to the ocean and in another case, swell energy is lost to the atmosphere. Babanin (2011) argues that interaction between swells and ocean turbulence is the primary mechanism producing swell attenuation. This concept forms the basis for the ZET15 parameterization for swell dissipation. In this case, the existence of swell energy results in a local increase of TKEF to the ocean. The ZET15 parameterization is used to calculate TKEF increase due to Southern Ocean swells. No correlations are found between this TKEF increase and SST anomaly in either the Niño-3 region or the Indian Ocean.

With the AET10 parameterization, swells are dissipated by a flux of energy to the atmosphere. This result is the same as for the ZET15 parameterization; however, the dissipation of swell energy by AET10 is found to not correlate with SST anomalies.

Differences appear to be in the wind sea. Both ZET15 and AET10 source functions, though they are implemented for the purpose of reproducing observed decay of swell energy, may act on all wave components (i.e., including wind-sea elements). However, these two parameterizations behave differently for nonbreaking dissipation. While the AET10 parameterization produces a damping of short wind waves due to the presence of Southern Ocean swells, the ZET15 parameterization is strictly local in frequency space, meaning that swells can have no direct effect on local wind seas via this source function.

In the case of AET10, loss of wind-sea energy to the atmosphere results in a reduction of TKE flux to the ocean, and this reduction is enhanced in cases where swell is present via the orbital velocity term: The presence of swells will increase the orbital velocity u_{orb} in the wave field, which will lead to a slight decrease of wind-sea energy and significant reduction in breaking and dissipation at high frequencies, hence reducing the TKEF. Thus, the TKEF reduction calculated using this parameterization is dominated by wind-sea damping due to swells.

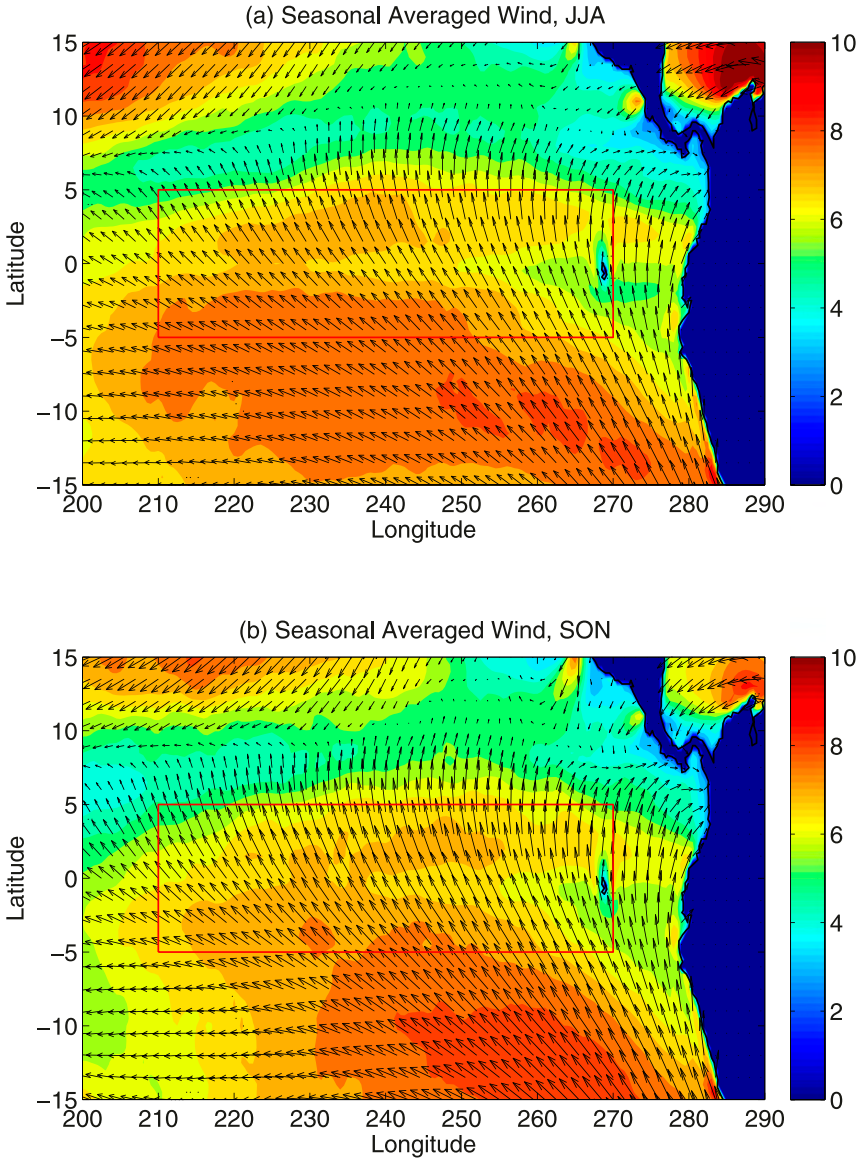

FIG. A1. Seasonal averaged wind speed (color, m s^{-1}) and direction (arrows) for (a) JJA and (b) SON.

In the Niño-3 region, the AET10 simulations give an average of 3%–4% TKEF reduction with maximum of 40%–50% reduction in some areas on the eastern part of the region. The TKEF reduction anomaly is found to be in opposite phase with the SST anomaly. In other words, a significant correlation is found. It is beyond the scope of the present study to establish a causal link. However, it is worth noting that if Southern Ocean swells play a significant role in regulating the SST anomalies in the Niño-3 region and the southeastern Indian Ocean, such a correlation would be expected.

The bimonthly averaged TKEF reduction in the southeastern Indian Ocean is found to be well correlated with the SST dipole mode suggested by Saji et al. (1999). The reduction reaches 5% during positive Indian Ocean dipole (IOD) years (2006–08) and become much weaker in non-IOD years (2004, 2005, and 2009).

Since the AET10 dissipation has a cumulative behavior (i.e., wind-sea dissipation depends on swell), the swell influence on the local wave climate is what provides the link with the SST variations rather than the swell dissipation itself. Therefore, if there are correlated changes to the winds at high latitudes that produce the swells, and at low latitudes that produce the local wind seas, correlated changes to SST can be expected.

Acknowledgments. The authors would like to express their appreciation to Drs. Fabrice Ardhuin, Luigi Cavaleri, Hector García-Nava, Dr. Alexander Babanin, and the anonymous reviewers for very helpful comments and suggestions. We thank the WAVEWATCH III development team for developing the code used in this study. NOAA/NWS/EMC/WAVEWATCH III public release version 4.18 is used to generate the data for this study. The wind and ice data used to force the model are available from NOAA/NCEP Climate Forecast System Reanalysis (datasets are named wnd10m.gdas.yyyymm.grb2 and icecon.gdas.yyymm.grb2). This work was funded by the Office of Naval Research under program element 0602435N. This paper is contribution NRL/JA/7320-15-2622 and has been approved for public release.

APPENDIX

Seasonal Mean Winds in the Niño-3 Region

To determine the right wind magnitude and direction to use in the uniform wind experiment in section 3, we calculate the mean of wind vectors in the Niño-3 region for the JJA and SON seasons (Fig. A1). The mean wind speed varies from 5 to 8 m s^{-1} in the domain. The mean wind direction is roughly northward in the eastern one-third of the Niño-3 box, especially along the eastern boundary of the box, where the changes to WAMF and TKEF are the strongest. Since the temporal varying wind could have larger or smaller magnitude than the mean, and wind directions also changes with time, for simplicity it is reasonable to use northward winds with magnitude of 5–10 m s^{-1} in the idealized experiment.

REFERENCES

Alves, J. H., 2006: Numerical modeling of ocean swell contributions to the global wind-wave climate. *Ocean Modell.*, **11**, 98–122, doi:10.1016/j.ocemod.2004.11.007.

Ardhuin, F., and Coauthors, 2010: Semiempirical dissipation source functions for ocean waves. Part I: Definition, calibration, and validation. *J. Phys. Oceanogr.*, **40**, 1917–1941, doi:10.1175/2010JPO4324.1.

Babanin, A. V., 2006: On a wave-induced turbulence and a wave-mixed upper ocean layer. *Geophys. Res. Lett.*, **33**, L20605, doi:10.1029/2006GL027308.

——, 2011: *Breaking and Dissipation of Ocean Surface Waves.* Cambridge University Press, 480 pp.

Behera, S. K., and T. Yamagata, 2001: Subtropical SST dipole events in the southern Indian Ocean. *Geophys. Res. Lett.*, **28**, 327–330, doi:10.1029/2000GL011451.

Bjerknes, J., 1966: A possible response of the atmospheric Hadley circulation to equatorial anomalies of ocean temperature. *Tellus*, **18**, 820–829, doi:10.1111/j.2153-3490.1966.tb00303.x.

Cai, W., A. Sullivan, and T. Cowan, 2009: How rare are the 2006–2008 positive Indian Ocean dipole events? An IPCC AR4 climate model perspective. *Geophys. Res. Lett.*, **36**, L08702, doi:10.1029/2009GL037982.

Cavaleri, L., B. Fox-Kemper, and M. Hemer 2012: Wind waves in the coupled climate system. *Bull. Amer. Meteor. Soc.*, **93**, 1651–1661, doi:10.1175/BAMS-D-11-00170.1.

Cherchi, A., and A. Navarra, 2013: Influence of ENSO and of the Indian Ocean dipole on the Indian summer monsoon variability. *Climate Dyn.*, **41**, 81–103, doi:10.1007/s00382-012-1602-y.

Donelan, M. A., 1987: The effect of swell on the growth of wind wave. *Johns Hopkins APL Tech. Dig.*, **8**, 18–23.

——, W. M. Drennan, and K. B. Kasaros, 1997: The air–sea momentum flux in conditions of wind sea and swell. *J. Phys. Oceanogr.*, **27**, 2087–2099, doi:10.1175/1520-0485(1997)027<2087:TASMFI>2.0.CO;2.

Drennan, W. M., K. K. Kahma, and M. A. Donelan, 1999: On momentum flux and velocity spectra over waves. *Bound.-Layer Meteor.*, **92**, 489–515, doi:10.1023/A:1002054820455.

Fan, Y., and S. M. Griffies, 2014: Impacts of parameterized Langmuir turbulence and nonbreaking wave mixing in global climate simulations. *J. Climate*, **27**, 4752–4775, doi:10.1175/JCLI-D-13-00583.1.

——, I. Ginis, and T. Hara, 2009: The effect of wind–wave–current interaction on air–sea momentum fluxes and ocean response in hurricanes. *J. Phys. Oceanogr.*, **39**, 1019–1034, doi:10.1175/2008JPO4066.1.

——, ——, and ——, 2010: Momentum flux budget across air–sea interface under uniform and tropical cyclone winds. *J. Phys. Oceanogr.*, **40**, 2221–2242, doi:10.1175/2010JPO4299.1.

——, S.-J. Lin, I. M. Held, Z. Yu, and H. L. Tolman, 2012: Global ocean surface wave simulation using a coupled atmosphere–wave model. *J. Climate*, **25**, 6233–6252, doi:10.1175/JCLI-D-11-00621.1.

——, ——, S. M. Griffies, and M. A. Hemer, 2014: Simulated global swell and wind-sea climate and their responses to anthropogenic climate change at the end of the twenty-first century. *J. Climate*, **27**, 3516–3536, doi:10.1175/JCLI-D-13-00198.1.

García-Nava, H., F. J. Ocampo-Torres, P. Osuna, and M. A. Donelan, 2009: Wind stress in the presence of swell under moderate to strong wind conditions. *J. Geophys. Res.*, **114**, C12008, doi:10.1029/2009JC005389.

——, ——, P. A. Hwang, and P. Osuna, 2012: Reduction of wind stress due to swell at high wind conditions. *J. Geophys. Res.*, **117**, C00J11, doi:10.1029/2011JC007833.

Grachev, A. A., and C. W. Fairall, 2001: Upward momentum transfer in the marine boundary layer. *J. Phys. Oceanogr.*, **31**, 1698–1711, doi:10.1175/1520-0485(2001)031<1698:UMTITM>2.0.CO;2.

——, ——, J. E. Hare, J. B. Edson, and S. D. Miller, 2003: Wind stress vector over ocean waves. *J. Phys. Oceanogr.*, **33**, 2408–2429, doi:10.1175/1520-0485(2003)033<2408:WSVOOW>2.0.CO;2.

Hanley, K. E., and S. E. Belcher, 2008: Wave-driven wind jets in the marine atmospheric boundary layer. *J. Atmos. Sci.*, **65**, 2646–2660, doi:10.1175/2007JAS2562.1.

Harris, D. L., 1966: The wave-driven wind. *J. Atmos. Sci.*, **23**, 688–693, doi:10.1175/1520-0469(1966)023<0688:TWDW>2.0.CO;2.

Huang, C. J., F. Qiao, Z. Song, and T. Ezer, 2011: Improving simulations of the upper ocean by inclusion of surface waves in the Mellor–Yamada turbulence scheme. *J. Geophys. Res.*, **116**, C01007, doi:10.1029/2010JC006320.

——, ——, Q. Shu, and Z. Song, 2012: Evaluating austral summer mixed-layer response to surface wave–induced mixing in the Southern Ocean. *J. Geophys. Res.*, **117**, C00J18, doi:10.1029/2012JC007892.

Ichiye, T., and J. Petersen, 1963: The anomalous rainfall of the 1957-58 winter in the equatorial central Pacific arid area. *J. Meteor. Soc. Japan*, **41**, 172–182.

Jensen, T. G., 2007: Wind-driven response of the northern Indian Ocean to climate extremes. *J. Climate*, **20**, 2978–2993, doi:10.1175/JCLI4150.1.

Kudryavtsev, V. N., and V. K. Makin, 2004: Impact of swell on the marine atmospheric boundary layer. *J. Phys. Oceanogr.*, **34**, 934–949, doi:10.1175/1520-0485(2004)034<0934:IOSOTM>2.0.CO;2.

Li, M., and C. Garrett, 1997: Mixed layer deepening due to Langmuir circulation. *J. Phys. Oceanogr.*, **27**, 121–132, doi:10.1175/1520-0485(1997)027<0121:MLDDTL>2.0.CO;2.

Makin, V. K., 2008: On the possible impact of a following-swell on the atmospheric boundary layer. *Bound.-Layer Meteor.*, **129**, 469–478, doi:10.1007/s10546-008-9320-z.

McWilliams, J. C., and P. P. Sullivan, 2000: Vertical mixing by Langmuir circulations. *Spill Sci. Technol. Bull.*, **6**, 225–237, doi:10.1016/S1353-2561(01)00041-X.

Murtugudde, R., J. P. McCreary Jr., and A. J. Busalacchi, 2000: Oceanic processes associated with anomalous events in the Indian Ocean with relevance to 1997–1998. *J. Geophys. Res.*, **105** (C2), 3295–3306, doi:10.1029/1999JC900294.

Philander, S. G., 1990: *El Niño, La Niña, and the Southern Oscillation.* Academic Press, 293 pp.

Phillips, O. M., and M. L. Banner, 1974: Wave breaking in the presence of wind drift and swell. *J. Fluid Mech.*, **66**, 625–640, doi:10.1017/S0022112074000413.

Qiao, F., Y. Yuan, Y. Yang, Q. Zheng, C. Xia, and J. Ma, 2004: Wave-induced mixing in the upper ocean: Distribution and application to a global ocean circulation model. *Geophys. Res. Lett.*, **31**, L11303, doi:10.1029/2004GL019824.

——, ——, T. Ezer, C. Xia, Y. Yang, X. Lu, and Z. Song, 2010: A three-dimensional surface wave–ocean circulation coupled model and its initial testing. *Ocean Dyn.*, **60**, 1339–1355, doi:10.1007/s10236-010-0326-y.

Rasmusson, E. M., and T. H. Carpenter, 1982: Variations in tropical sea surface temperature and surface wind fields associated with the Southern Oscillation–El Niño. *Mon. Wea. Rev.*, **110**, 354–384, doi:10.1175/1520-0493(1982)110<0354:VITSST>2.0.CO;2.

Saha, S., and Coauthors, 2010: The NCEP Climate Forecast System Reanalysis. *Bull. Amer. Meteor. Soc.*, **91**, 1015–1057, doi:10.1175/2010BAMS3001.1.

Saji, N. H., B. N. Goswami, P. N. Vinayachandran, and T. Yamagata, 1999: A dipole mode in the tropical Indian Ocean. *Nature*, **401**, 360–363.

Sloyan, B. M., G. C. Johnson, and W. S. Kessler, 2003: The Pacific cold tongue: A pathway for interhemisphere exchange. *J. Phys. Oceanogr.*, **33**, 1027–1043, doi:10.1175/1520-0485(2003)033<1027:TPCTAP>2.0.CO;2.

Smyth, W. D., E. D. Skyllingstad, G. B. Grawford, and H. Wijesekera, 2002: Nonlocal fluxes and Stokes drift effects in the K-profile parameterization. *Ocean Dyn.*, **52**, 104–115, doi:10.1007/s10236-002-0012-9.

Sullivan, P. P., J. B. Edson, T. Hristov, and J. C. McWilliams, 2008: Large-eddy simulations and observations of atmospheric marine boundary layers above nonequilibrium surface waves. *J. Atmos. Sci.*, **65**, 1225–1245, doi:10.1175/2007JAS2427.1.

Tolman, H. L., 2003: Treatment of unresolved islands and ice in wind wave models. *Ocean Modell.*, **5**, 219–231, doi:10.1016/S1463-5003(02)00040-9.

——, and Coauthors, 2014: User manual and system documentation of WAVEWATCH III version 4.18. NOAA, 311 pp. [Available online at http://polar.ncep.noaa.gov/waves/wavewatch/manual.v4.18.pdf.]

Webster, P. J., A. M. Moore, J. P. Loschnigg, and R. R. Leben, 1999: Coupled ocean–atmosphere dynamics in the Indian Ocean during 1997–98. *Nature*, **401**, 356–360, doi:10.1038/43848.

Wyrtki, K., 1981: An estimate of equatorial upwelling in the Pacific. *J. Phys. Oceanogr.*, **11**, 1205–1214, doi:10.1175/1520-0485(1981)011<1205:AEOEUI>2.0.CO;2.

Young, I. R., A. Babanin, and S. Zieger, 2013: The decay rate of ocean swell observed by altimeter. *J. Phys. Oceanogr.*, **43**, 2322–2333, doi:10.1175/JPO-D-13-083.1.

Zieger, S., A. V. Babanin, W. E. Rogers, and I. R. Young, 2015: Observation-based source terms in the third-generation wave model WAVEATCH. *Ocean Modell.*, doi:10.1016/j.ocemod.2015.07.014, in press.